Investigation of Iron Dissolution Mechanism in Acidic Solutions with and without Dissolved CO_2—Part I: Electrochemical Impedance Spectroscopy Measurements

Negar Moradighadi,[*] Huiru Wang,[*] Luntao Wang,[,***] Antoine Seyeux,[**] Alain Pailleret,[***] Philippe Marcus,[**] and Srdjan Nesic[‡,*]*

Aqueous CO_2 corrosion of mild steel is one of the major problems in the oil and gas industry. While current understanding primarily focuses on cathodic reaction mechanisms, less attention has been given to the impact of aqueous CO_2 on the anodic iron dissolution reaction. In contrast, the mechanism of iron dissolution in strongly acidic environments has been thoroughly investigated. Among the reaction mechanisms found in the open literature, a multipath mechanism was identified that could explain the iron dissolution in strong acidic sulfate solution; both in terms of steady-state polarization sweeps and impedance data at various pH values and current densities. However, the role of aqueous CO_2 in solutions containing chlorides on the mechanism of iron dissolution remained an open question. The present study used electrochemical impedance spectroscopy (EIS) as the main technique, to study the mechanism of iron dissolution in strong acid chloride solution with and without the presence of CO_2. Results showed that the presence of chloride ions (0.5 M) decreased the rate of iron dissolution by competing with hydroxide ions to adsorb on the metal surface, forming chloride-containing intermediate species that participate in the iron dissolution reaction. The resulting decrease in the availability of hydroxide intermediates, which are more effective at enhancing the reaction rate compared to chloride-containing intermediates, leads to an overall decrease in the rate of iron dissolution. While the presence of CO_2 increases anodic current density, EIS investigation revealed that neither aqueous CO_2 nor other carbonic species directly react on the bare metal surface to form adsorbed intermediates involved in the anodic reaction. EIS investigation suggested that aqueous CO_2 may induce changes in the chemical composition of adsorbed species, rate constants, and surface coverage, thereby altering the kinetics of the underlying reactions.

KEY WORDS: anodic polarization, carbon dioxide, electrochemical impedance spectroscopy, polarization, sodium chloride

INTRODUCTION

In the oil and gas pipelines, and other equipment made from mild steel, the presence of CO_2 dissolved in an aqueous environment plays a critical role in corrosion mechanisms. Understanding how anodic iron dissolution happens along with cathodic reaction mechanisms in such environments helps to develop mechanistic models to predict the corrosion rate in a broad range of environments. The cathodic reaction, which mainly involves hydrogen reduction (Reaction [1]) is an important element of the overall corrosion mechanism and has been intensely studied in the past few decades.[1] The present study will focus on elucidating the mechanism of the anodic iron dissolution, with Reaction (2) being the overall reaction.

$$2H^{+}_{(aq)} + 2e^{-} \rightleftarrows H_{2(g)} \quad (1)$$

$$Fe_{(s)} \rightleftarrows Fe^{2+}_{(aq)} + 2e^{-} \quad (2)$$

A simple analysis reveals that an elementary (single-step) reaction is unlikely. For this to happen, a surface $Fe_{(s)}$ atom would have to be oxidized by simultaneously releasing two electrons, which from a statistical mechanics point of view is very improbable. There are other ways of proving the same point, for example: the rate of the iron dissolution reaction is found to be pH-dependent, which could not be the case if it occurred in a single step as represented by Reaction (2) without any hydrogen or hydroxide ions involved.[2]

As will be shown below, the present work primarily builds on the well-known electrochemical impedance spectroscopy (EIS) study of Keddam, et al., published in 1981, who proposed a multipath mechanism for iron dissolution including three parallel dissolution paths based on results of both steady-state polarization and EIS measurements.[3-4] Their study was conducted in strong acid sulfate solutions and mostly at lower compared to that of interest in CO_2 corrosion of mild steel. The role of chlorides (almost always present in CO_2 corrosion of mild steel) and aqueous CO_2 and other carbonic species,

Submitted for publication: December 26, 2023. Revised and accepted: May 04, 2024. Preprint available online: May 08, 2024, https://doi.org/10.5006/4511.
‡ Corresponding author. E-mail: nesic@ohio.edu.
* Institute for Corrosion and Multiphase Technology, Ohio University, Athens Ohio 45701.
** Université PSL, CNRS – Chimie ParisTech, Institut de Recherche de ChimieParis, Groupe Physico-Chimie des Surfaces, 75005 Paris, France.
*** Sorbonne Université, CNRS, Laboratoire Interfaces et Systèmes Electrochimiques, 75005, Paris, France.

ISSN 0010-9312 (print), 1938-159X (online)

on the kinetics of the anodic reaction is poorly understood. Some previous studies (discussed further below) found no differences between anodic potentiodynamic sweeps, conducted in the absence and presence of aqueous CO_2 close to the open-circuit potential (i.e., in the active dissolution range), and therefore concluded that CO_2 does not affect the mechanism and rate of the iron dissolution reaction.[5-8] There is another group of researchers that found that CO_2 affects iron dissolution and increases the reaction rate, particularly at more positive potential ranges such as transition and prepassivation regions.[9-11]

Therefore, the question addressed in the present study is: what is the effect of chlorides and carbonic species in aqueous CO_2 solutions on the mechanism and rate of iron dissolution? Both DC (potentiodynamic sweeps) and AC measurements, i.e., EIS, were used to study the role of chlorides and CO_2 on the mechanism of the iron dissolution and compare it to that in strongly acidic solution, similarly as was done in the original study of Keddam, et al.[3-4] A parallel study using time-of-flight secondary ion mass spectroscopy (TOF-SIMS) was conducted on the same subject and is published as Part II of this paper series.[12]

BACKGROUND

El Miligy, et al., categorized the various mechanisms of dissolution of iron according to four potential ranges based on steady-state polarization curves; namely active dissolution, transition, prepassivation, and passivation, as illustrated in Figure 1.[13] In corrosion of mild steel in aqueous CO_2 solutions, the primary interest is in the potential range close to the OCP. This range encompasses the active dissolution region, where significant corrosion occurs. Although transition and prepassivation mechanisms are usually of lesser significance, they may still influence corrosion behavior under specific conditions. For instance, when the corrosion potential reaches the potential range where the rate of anodic reaction is in the transition and prepassivation region, these mechanisms become directly relevant.

For the active dissolution range, Heusler[14] proposed the "self-catalytic mechanism" based on the experimentally

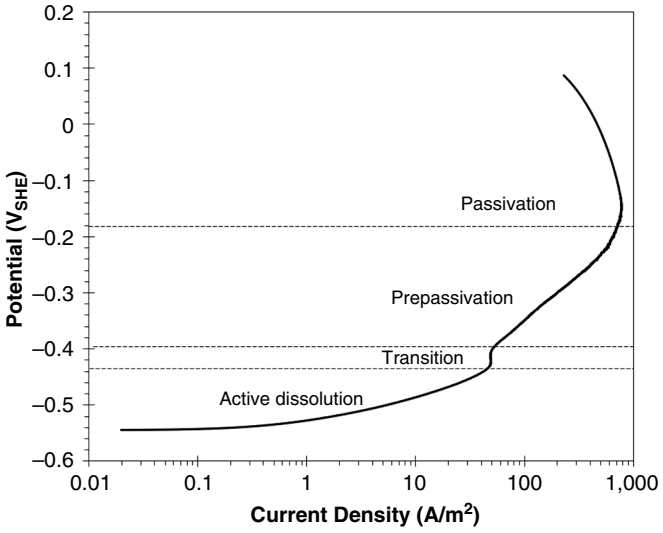

FIGURE 1. *Anodic dissolution of iron in 0.5 M NaCl, pH 6.0, 25°C, 1 bar CO_2, using rotating disk pure iron electrode at 1,600 rpm and a scan rate of 0.5 mV/s: classification of graph regions according to El Miligy, et al.*[13]

observed Tafel slope of 30 mV/decade and an order of reaction with respect to pH of −2. This mechanism consists of two sets of parallel iron dissolution reactions. In the first sequence (Reactions [3] through [5]), which does not consume a lot of iron and produces little current, a catalytic species is formed. It starts with water adsorbed on the iron surface which then leads to the formation of an adsorbed iron-hydroxide ion intermediate $Fe(OH^-)_{(ads)}$, which is subsequently oxidized to form an adsorbed intermediate $FeOH_{(ads)}$ that acts as a catalyst in the second and main set of iron dissolution reactions.

$$Fe_{(s)} + H_2O_{(l)} \rightleftarrows Fe(H_2O)_{(ads)} \quad (3)$$

$$Fe(H_2O)_{(ads)} \rightleftarrows Fe(OH^-)_{(ads)} + H^+_{(aq)} \quad (4)$$

$$Fe(OH^-)_{(ads)} \rightleftarrows (FeOH)_{(ads)} + e^- \quad (5)$$

Adding Reactions (3) through (5) gives Reaction (6) and this is how the initial catalyst-forming step in Heusler's "self-catalytic mechanism" is often shown compactly.

$$Fe_{(s)} + H_2O_{(l)} \rightleftarrows FeOH_{(ads)} + H^+_{(aq)} + e^- \quad (6)$$

According to Heusler, Reactions (7) through (9) are the second and main sequence of iron dissolution reactions that produce most of the anodic current. It is important to mention that in this sequence, the rate-determining step (rds) Reaction (8) is not a true elementary reaction step, as it shows that two electrons are transferred simultaneously, which is very improbable and is not consistent with the electrochemical theory describing elementary reactions, as discussed above.

$$Fe_{(s)} + FeOH_{(ads)} \rightleftarrows Fe(FeOH)_{(ads)} \quad (7)$$

$$Fe(FeOH)_{(ads)} + OH^-_{(aq)} \xrightarrow{rds} (FeOH)^+_{(aq)} + FeOH_{(ads)} + 2e^- \quad (8)$$

$$(FeOH)^+_{(aq)} \rightleftarrows Fe^{2+}_{(aq)} + OH^-_{(aq)} \quad (9)$$

Experiments conducted by Bockris, et al., showed a Tafel slope of 40 mV/decade and an order of reaction with respect to pH of −1.[2] The authors (Bockris, Despic, and Drazic) proposed a mechanism later called the "BDD mechanism" or "consecutive mechanism", which is represented by Reactions (10) through (12). This reaction sequence starts the same way as Heusler's mechanism, shown by Reactions (3) through (5), which is the same as Reaction (10) in the consecutive BDD mechanism. However, in the BDD mechanism, $FeOH_{(ads)}$ is not a "side-show" and does not act as a catalyst in some parallel reaction pathway that produces most of the anodic current, rather, it takes the "main stage," and is further oxidized in a consecutive single-electron transfer step, via the rate-determining Reaction (11). The last chemical step (12) in the BDD mechanism is again the same as Reaction (9) in Heusler's mechanism.

$$Fe_{(s)} + OH^-_{(aq)} \rightleftarrows FeOH_{(ads)} + e^- \quad (10)$$

$$FeOH_{(ads)} \xrightarrow{rds} (FeOH)^+_{(aq)} + e^- \quad (11)$$

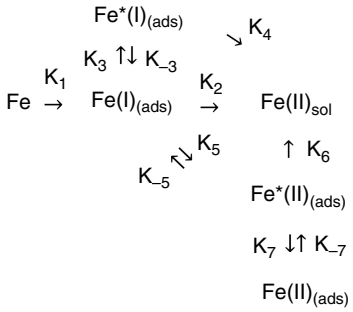

K_4 reaction:

$$Fe^*(I)_{(ads)} + Fe \xrightarrow{K_4} Fe^*(I)_{(ads)} + Fe(II)_{sol} + 2e^-$$

K_6 reaction:

$$Fe^*(II)_{(ads)} + Fe \xrightarrow{K_6} Fe^*(II)_{(ads)} + Fe(II)_{sol} + 2e^-$$

FIGURE 2. *Original multipath mechanism for iron dissolution from Keddam, et al.*[3]

$$(FeOH)^+_{(aq)} \rightleftarrows Fe^{2+}_{(aq)} + OH^-_{(aq)} \quad (12)$$

Both of these iron dissolution mechanisms, self-catalytic (Heusler) and consecutive (BDD), were obtained based on steady-state polarization curves near the OCP; assuming that each elementary step follows the Tafel law with a charge transfer coefficient of 0.5.[2,14] Years later, Epelboin and Keddam showed that the experimental impedance data of iron dissolution near the OCP has a high-frequency capacitive loop associated to the double layer capacitance in parallel with a charge transfer resistance and a low-frequency inductive loop related to the adsorbed hydroxide intermediates, which seemed consistent with both the catalytic (Heusler) and the consecutive (BDD) mechanisms.[15] However, when modeling the consecutive (BDD) mechanism, they illustrated that the resulting impedance spectra near the OCP show only one capacitive loop, which was not consistent with the experimental data obtained in that potential range. Therefore, they questioned some of the assumptions behind the consecutive (BDD) mechanism such as that the first oxidation step forming $FeOH_{(ads)}$ (Reaction [10]) is in near-equilibrium. The argument was that in the active dissolution range (close to the OCP), the potential is so much more positive compared to the reversible potential for this reaction, that the reverse reduction reaction is negligible. They also questioned the practice of using a charge transfer coefficient value of 0.5 for all elementary steps, as based on electrochemical theory, the charge transfer coefficient for an elementary reaction step can take any value between zero and one.[16] After revising the assumptions for the consecutive (BDD) mechanism, Epelboin and Keddam successfully modeled the impedance response of the anodic dissolution of iron near the open circuit potential.[15]

In a key 1981 study, Keddam, et al., looked into the mechanisms of iron dissolution, this time at different pH values and over a much broader range of potentials, using steady-state polarization sweeps and EIS measurements.[3-4] In the original mechanism proposed in that study, reproduced in Figure 2, there are three parallel iron dissolution paths. These three paths are here reconstructed in Figure 3, which we will use to argue that they include the equivalents of the BDD mechanism (as path 1), Heusler mechanisms (as path 2), and an additional path 3. The kinetic constants K for the reaction steps were defined using Equation (13)[(1)].

$$K_n = K_{n,0}\exp\left(\frac{z\,\alpha_n\,FE}{RT}\right) \quad (13)$$

The first step in all three paths proposed by Keddam, et al., is a pH-dependent oxidation reaction in which a monovalent iron adsorbed intermediate $Fe(I)_{(ads)}$ is formed.[3-4] Even if Keddam, et al., do not indicate its composition, by comparing with the first step in the Heusler[14] and Bockris, et al.,[2] mechanisms, we can deduce that $Fe(I)_{(ads)}$ is likely to be $FeOH_{(ads)}$[(2)]. In the next steps, the $Fe(I)_{(ads)}$ participates in three different parallel reaction paths.

Path 1 is assumed to be the most significant one in the active dissolution region. If we consider that Keddam, et al.,'s bivalent iron compound $Fe(II)_{(aq)}$ shown in this path could actually be $(FeOH)^+_{(aq)}$, then path 1 is similar to the BDD consecutive mechanism represented by Reactions (10) and (11), with the distinction of the first step being considered by Keddam, et al.,[3-4] to be irreversible, rather than in near-equilibrium, as Bockris, et al., assumed.[2]

Path 2 of Keddam, et al.,'s multipath mechanism, prominent at more positive potentials, is similar to the Heusler self-catalytic mechanism, Reactions (7) and (8). In this path, following the common first step where $Fe(I)_{(ads)}$ is formed, it then transforms into a catalytic surface species $Fe(I)^*_{(ads)}$[(3)]. When compared to the second step of Heusler's mechanism (Reaction [7]), we can speculate that $Fe(I)^*_{(ads)}$ might be $Fe(FeOH)_{(ads)}$. In the main rate-determining reaction that follows, the iron atom is oxidized with the simultaneous release of two electrons, just as Heusler suggested by Reaction (8). One can level the same criticism here as when discussing Heusler's-mechanism, that this cannot be an elementary reaction. There is one difference between the Heusler self-catalytic mechanism and Keddam, et al.'s path 2—the formation of a catalytic species $Fe(I)^*_{(ads)}$ is through a chemical reaction which according to Keddam, et al., "may be potential dependent".[3] Although general chemical rate theory suggests that a nonredox chemical reaction such as the one considered here cannot depend on potential, Keddam, et al., used this assumption to better fit the model to the experimental polarization sweeps and EIS data.

Path 3 of multipath mechanism, also prominent at potentials more positive than the OCP, includes the common first step, where $Fe(I)_{ads}$ is formed, followed by the formation of

(1) In this study, $K_{n,0}$ refers to the rection rate at E = 0 relative to the equilibrium potential. z represents the number of electrons and α_n denotes the charge transfer coefficient. Additionally, F, R, and T stand for the Faraday constant, universal gas constant, and temperature.

(2) The three parallel iron dissolution paths in Keddam, et al., mechanism include the three adsorbed intermediate species: $Fe(I)_{(ads)}$, $Fe^*(I)_{(ads)}$, and $Fe^*(II)_{(ads)}$, what seems like an unusual notation.[3-4] It is true that in most cases, we do not have explicit independent evidence about the exact composition of the adsorbed intermediate species. Hence, Keddam, et al., notation, where they chose only to indicate the iron oxidation state of the adsorbed intermediates using the Roman numerals, seems appropriate. On the other hand, it is more common and one can argue—more intuitive, to use the exact chemical notation as used by Heusler[14] and Bockris, et al.,[2] even if this includes some degree of speculation. We will here try and take a middle ground by showing both notations.

(3) Star sign (*) in Keddam, et al.,'s multipath mechanism indicates that the adsorbed intermediate acts as a catalyst in the following reaction steps.

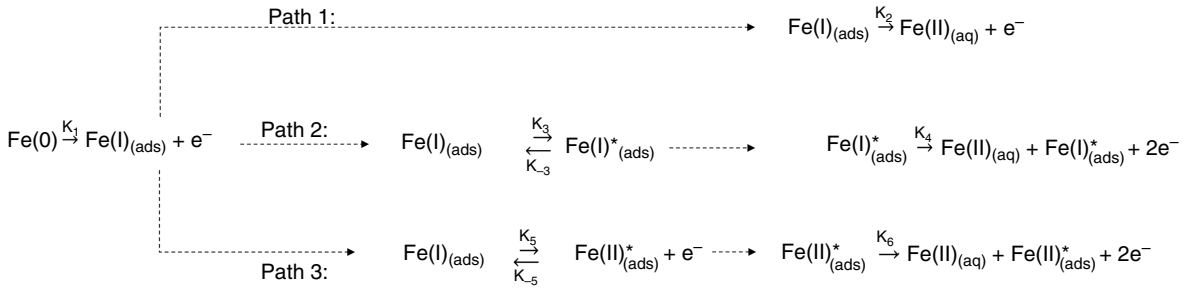

FIGURE 3. *Reconstructed multipath mechanism for iron dissolution following the original scheme of Keddam, et al.,[3] shown in Figure 2 (and by ignoring the passivation step).*

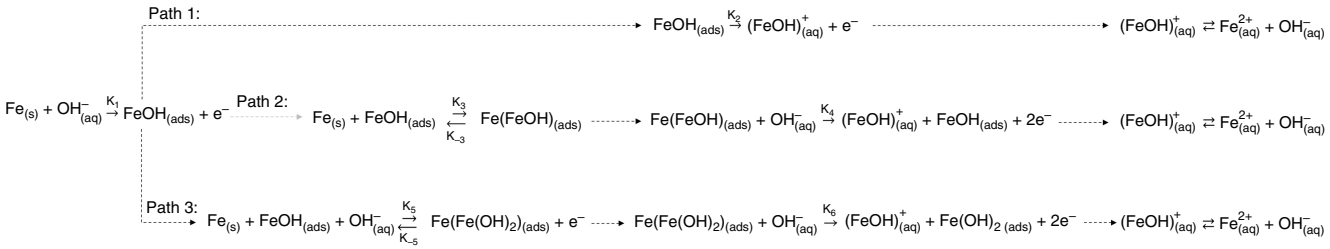

FIGURE 4. *Translated multipath mechanism for iron dissolution following Keddam, et al.,[3-4] shown in Figure 3, using equivalent species with an exact chemical composition deduced by analogy with the consecutive (BDD)[2] and catalytic (Heusler) mechanisms.[14]*

another catalytic species, this time a bivalent iron intermediate $Fe(II)^{*}_{ads}$. By analogy with the path 2, we can deduce that $Fe(II)^{*}_{(ads)}$ could be $Fe(Fe(OH)_2)_{(ads)}$. Path 3 is otherwise very similar to path 2, with the second step being the main iron-dissolving reaction with a two-electron transfer. At even more positive potentials, the passivation of iron happens by the formation of $Fe(II)_{(ads)}$ (refer to Figure 2), which is not of high interest in the present study which is focused on the corrosion of steel in acidic solutions.

If we now "translate" Keddam, et al.,'s multipath mechanism shown in Figure 3 and introduce species with an exact chemical composition, deduced by analogy with the consecutive (BDD) and catalytic (Heusler) mechanisms, and write stoichiometrically correct reaction steps, the resulting scheme is shown in Figure 4 (it does not include the passivation step which is of little interest here). It should be stressed again that this "translation" exercise includes a certain degree of speculation and uncertainty, however, it enables us to better connect Keddam, et al.,'s multipath scheme with the previously proposed consecutive (BDD) and catalytic mechanisms for iron dissolution in strongly acidic aqueous solutions. It also forms a solid basis for expanding Keddam, et al.,'s multipath scheme to include the effects of chloride and carbonic species present in aqueous CO_2 solutions.

As an illustration of how these three paths for iron dissolution come together in the Keddam, et al., model, Figure 5 shows an example of how we reconstructed an anodic polarization sweep at pH 5 in a strongly acid sulfate solution, using their kinetic parameters.[3-4] Here, the total iron dissolution current density is obtained as a sum of the three partial current densities corresponding to the three paths.

In this example, path 1 is dominant closer to the OCP, with path 3 "taking over" at more positive potentials and path 2 being insignificant under these conditions. The reason that each path results in an initial increase of the iron dissolution current with potential, followed by a peak and a decrease, is due to competing surface coverages by the various adsorbed intermediates associated with these paths. In the example shown in Figure 5, the interplay of path 1 and path 3 results in the S-shape polarization curve, seen closer to the OCP. The larger S-shape curve obtained at more positive potentials is due to the onset of passivation.

We need to recall that the Keddam, et al.,[3-4] study, while being comprehensive and convincing, was conducted in strong acid sulfate solutions, and the question that needs to be answered now is, was there any specific influence of the anion type (sulfate) on the iron dissolution mechanism and rate, and would the results be different in a different solution, say one that

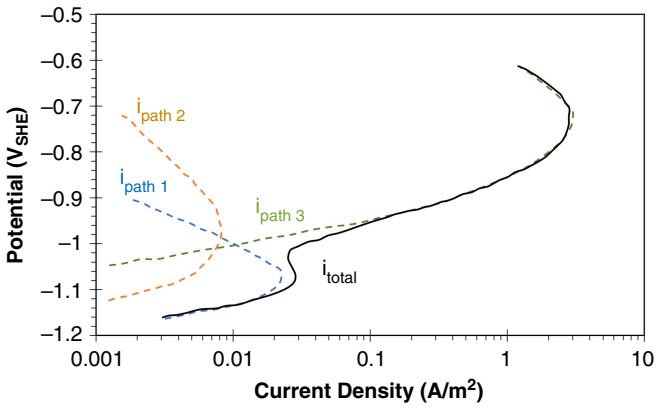

FIGURE 5. *Reconstructed anodic polarization sweep using Keddam, et al., data and following their multipath mechanism.[3-4] Model parameters: pH 5, 1 bar Ar, 25°C, 1 M Na_2SO_4, 1,600 rpm, RDE, pure iron (from Johnson-Matthey).*

contains chloride or carbonate anions (CO_2 solutions)? Those will be discussed next.

2.1 | Effect of Anion on the Mechanism of Iron Dissolution

There are several major findings reported in the literature regarding the role of anions in the mechanism of iron dissolution.[17-24] Among them, there are contradictory conclusions regarding the role of sulfate anions (SO_4^{2-}) on the mechanism of iron dissolution. There are papers indicating that SO_4^{2-} can participate in iron dissolution, while others indicate that it does not have an effect and can be considered as being inert when it comes to this reaction.[17,19] On the other hand, there seems to be a consensus that halide ions such as Cl^-, Br^-, and I^-, can partially displace adsorbed OH^-, at the iron surface through competitive adsorption and thereby affect iron dissolution.[17-18,20,23-24] In that scenario, some studies indicate that halides such as Cl^- can decelerate the anodic reaction while other studies reported the acceleration effect of Cl^- on the iron dissolution.[17,23-25]

The effect of iodide (I^-) on iron dissolution was discussed by Heusler and Cartledge.[20] The authors observed S-shaped anodic polarization curves indicating two Tafel slopes of 60 mV/decade at more negative potential and 30 mV/decade at more positive potential. Therefore, according to the authors, the anodic dissolution of iron proceeds through two parallel reactions producing a total current i_{total}, as shown by Equation (14).

$$i_{total} = i_1 + i_2 \tag{14}$$

where i_1 is the current density obtained from iron dissolution on the halide-free (hydroxide-covered) surface, where the Tafel slope is 30 mV/decade, and i_2 is the current density obtained on the iron surface covered by halide ions and is dominant at more negative potentials, where the Tafel slope is equal to 60 mV/decade. The contribution of each current is dependent on the surface coverage by halide ions. As halide ions adsorb on the iron surface and the surface coverage by the hydroxide ions decreases, consequently, the current density i_1 decreases, given that Heusler's catalytic effect becomes weaker.

Similar mechanisms were put forward subsequently, where it was suggested that the adsorbed halide ion compete with the hydroxide ions for coverage on the surface and then participate in the mechanism of the iron dissolution reaction. One proposal is the "halide inhibited" mechanism, shown by Reactions (15) through (19) below. There, the adsorbed iron-halide $Fe(X^-)_{(ads)}$ intermediates (where X^- is a generic halide anion) "interfere" with hydroxide-catalyzed oxidation of iron, which is represented as a two-electron transfer, Reaction (18)[17,23]

$$Fe_{(s)} + H_2O_{(l)} \leftrightarrow Fe(H_2O)_{(ads)} \tag{15}$$

$$Fe(H_2O)_{(ads)} \leftrightarrow Fe(OH^-)_{(ads)} + H^+_{(aq)} \tag{16}$$

$$Fe_{(s)} + X^-_{(aq)} \leftrightarrow Fe(X^-)_{(ads)} \tag{17}$$

$$Fe(OH^-)_{(ads)} + Fe(X^-)_{(ads)} \rightarrow Fe_{(s)} + (FeOH)^+_{(aq)} + X^-_{(aq)} + 2e^- \tag{18}$$

$$(FeOH)^+_{(aq)} + H^+_{(aq)} \leftrightarrow Fe^{2+}_{(aq)} + H_2O_{(l)} \tag{19}$$

The Kuo and Nobe mechanism suggests that iron dissolution behaves differently depending on the chloride ions concentration.[25] Above 0.005 M, chloride ions accelerate the rate of iron dissolution, while below this concentration, they inhibit it. Within the context of experiments conducted in a low acidic solution (pH 1.1), Kuo and Nobe's mechanism postulates the existence of two parallel pathways for iron dissolution: one pathway, dominant at higher anodic potential, involves acceleration by OH^- ions, following the consecutive (BDD) mechanism Reactions (10) through (12). The other pathway, active at lower anodic potential, is accelerated by Cl^- ions, leading to the formation of an adsorbed chloro-hydroxide iron intermediate, which is then reduced in two consecutive steps shown by Reactions (20) through (22).

$$Fe_{(s)} + OH^-_{(aq)} + Cl^-_{(aq)}(aq) \rightleftarrows (FeClOH)^-_{(ads)} + e^- \tag{20}$$

$$(FeClOH)^-_{(ads)} \xrightarrow{rds} FeClOH_{(ads)} + e^- \tag{21}$$

$$FeClOH_{(ads)} \rightleftarrows Fe^{2+}_{(aq)} + Cl^-_{(aq)} + OH^-_{(aq)} \tag{22}$$

MacFarlane and Smedley[22] proposed a mechanism for iron dissolution in 4.5 M chloride solution and a pH range of 0 to 4, based on two distinct Tafel slopes obtained at low and high current density, starting with the Kuo and Nobe[25] mechanism for chloride solutions and then introducing the Keddam, et al.,[3-4] multipath mechanism defined for sulfate solution. In their proposed mechanism, Reactions (23) through (26) bear similarities to the Kuo and Nobe mechanism, while Reactions (27) and (28) resemble path 2 of the Keddam, et al., mechanism. The difference is that in the Kuo and Nobe mechanism, the intermediate species $(FeClOH)^-_{(ads)}$ and $FeClOH_{(ads)}$ undergo a two-step oxidation process followed by a chemical reaction to release $Fe^{2+}_{(aq)}$, as illustrated in Reactions (20) through (22). In contrast, in the MacFarlane and Smedley mechanism, the chloride intermediate species is only $(FeClOH)^-_{(ads)}$, which undergoes a single-step oxidation to form $(FeOH)^+_{(aq)}$, as shown in Reactions (23) and (24), followed by a chemical reaction to yield $Fe^{2+}_{(aq)}$.

Within MacFarlane and Smedley's framework, Reactions (23) and (24) dominate at lower anodic potentials where $Fe(I)^1_{(ads)}$ and $Fe(I)_{(ads)}$ correspond to $(FeClOH)^-_{(ads)}$ and $FeOH_{(ads)}$, respectively. In addition, Reactions (25) through (28) (which are similar to the reactions in path 2 of the Keddam, et al., mechanism) become dominant at higher anodic potentials where $Fe(I)^*_{(ads)}$ represents a catalytic species.[22]

$$Fe \leftrightarrow Fe(I)^1_{(ads)} + e^- \tag{23}$$

$$Fe(I)^1_{(ads)} \rightarrow Fe(II)_{sol} + e^- \tag{24}$$

$$Fe \leftrightarrow Fe(I)_{(ads)} + e^- \tag{25}$$

$$Fe(I)_{(ads)} \rightarrow Fe(II)_{sol} + e^- \tag{26}$$

$$Fe(I)_{(ads)} \leftrightarrow Fe(I)^*_{(ads)} \tag{27}$$

$$Fe(I)^*_{ads} + Fe \rightarrow Fe(I)^*_{(ads)} + Fe(II)_{sol} + 2e^- \tag{28}$$

Further comparison of the mechanism for iron dissolution in sulfate and chloride solutions were published by Barcia and

Mattos.[21] They reported that the polarization curves in the low anodic current range were the same as those published by Keddam, et al.,[3-4] i.e., that there was no effect of chloride on the mechanism of the iron dissolution reaction. Apparently, according to EIS results, some integration of the chloride ions into the adsorbed intermediates was possible between pH 0 and pH 2, however, for pH ≥ 3, the same species, mechanisms, and kinetic constants are valid in chloride solutions as were they found in sulfate solutions by Keddam, et al. These findings are at odds with some of the other studies reported above. The justification offered by the authors was that at pH ≥ 3, the hydroxide ion is present at such high concentrations that it wins in the adsorption competition, and no effect of the type of ion is seen on anodic dissolution of iron. Due to this controversy, the effect of chloride on the mechanism and rate of iron dissolution will be reevaluated here.

2.2 | Effect of CO_2 on the Mechanism of Iron Dissolution

Even if iron dissolution in strong acidic environments has been the subject of many research studies, only a handful of them looked into the effect of aqueous CO_2 on the iron dissolution mechanisms, with varying results.[1,9-11,26-28] For example, Nesic, et al., reported that the effect of aqueous CO_2 is considerable in the active dissolution region, for CO_2 partial pressure in the range 0.2 bar < pCO_2 < 1 bar, where the surface coverage of steel by carbonic species was significant.[26] Apparently, for pCO_2 < 0.2 bar, the coverage was small and the effect negligible, while above pCO_2 >1 bar, no further changes were seen, as the surface coverage by carbonic species became saturated, the authors speculated.

In the studies published by Davies and Burstein and Linter and Burstein, the effect of CO_2 on the anodic dissolution of mild steel was also investigated.[9,11] Contrary to what was found by Nesic, et al.,[26] they showed that the presence of CO_2 did not affect the active dissolution region. However, it was reported that the presence of CO_2 increased the "first current maximum," and that its effect is noticeable in the transition and prepassivation potential range. They suggested that this effect of aqueous CO_2 is due to its interaction with the semipassive $Fe(OH)_2$ film resulting in the formation of iron complexes that are soluble in water.

Kahyarian, et al., studied the anodic dissolution of mild steel in the CO_2 aqueous environment.[10] They showed that the presence of CO_2 affects the mild steel dissolution in the active, transition, and prepassivation regions. In the active region, the presence of CO_2 decreased the Tafel slope from 28 mV/decade, in a solution without CO_2, to 22 mV/decade. Although this is a small difference, Kahyarian, et al., concluded that the mechanism of iron dissolution is different in the presence of CO_2. Almeida, et al.,[29] challenged this finding by arguing that different Tafel slopes cannot be used as a sole parameter to indicate different reaction mechanisms. They made the argument that Tafel slopes with similar values could potentially be associated with two different mechanisms. Furthermore, they suggested that the difference between the Tafel slopes of 22 mV and 28 mV in Kahyarian, et al., experimental results might be attributed to experimental errors rather than indicating the presence of two distinct mechanisms in the absence and presence of CO_2.

In 2017, Almeida, et al., performed EIS measurements to study the anodic reaction in strong acid solution and weak acidic CO_2 aqueous solutions at different pCO_2 values.[27] Experiments were performed without the presence of any supporting electrolyte and only at OCP, using a two-electrode experimental setup in which the electrodes were large and the distance between them small enough to minimize the effect of large solution resistance. Their results indicated that CO_2 does not have an effect on the mechanism of iron dissolution at OCP, under the conditions used in their experimentation.

Due to the contradictory findings regarding the effect of aqueous CO_2 on the anodic dissolution of iron reported in the literature, further investigation of the role of CO_2 on the mechanism of the anodic dissolution of iron was one of the primary objectives of the current study.

METHODOLOGY

EIS measurements were conducted in a three-electrode glass cell with a 99.99 wt% pure iron rotating disk working electrode (RDE) and saturated Ag/AgCl reference electrode. The graphite rod counter electrode was isolated in a glass chamber.[(4)] The 1 L test solution was a 0.3 M Na_2SO_4 or 0.5 M NaCl (research grade) aqueous solution which was continuously sparged with N_2 or CO_2 gas starting 1 h before the insertion of the RDE specimen into the solution[(5)]. The pH was adjusted before testing, using H_2SO_4 and NaOH for the sulfate-containing solution and HCl and NaOH for the chloride-containing solution. During testing, concentrated solutions of the respective chemicals were utilized for pH adjustment, and before use, these concentrated chemicals were deoxygenated. The temperature of the test solution was adjusted and maintained to 25±0.5°C using a hot plate before and during all electrochemical measurements. Before insertion into the solution, the RDE specimen surface was polished using 1200 grit silicon carbide abrasive papers and sonicated in an isopropyl alcohol bath, then dried using N_2 gas. The RDE rotation speed was adjusted to 1600 rpm using a modulated speed rotator.

Before a polarization experiment was initiated, OCP was monitored for at least 10 min and once the change in the OCP drift was less than 3 mV over 5 min, the experiment started. The steady-state potentiodynamic sweep measurements were performed by stepping the potential positively with respect to OCP using sweep rate of 0.125 mV/s or 0.5 mV/s. The data obtained using a sweep rate of 0.125 mV/s was proven to give reproducible results that did not differ from those obtained at 0.5 mV/s sweep rate speeds (Refer to Figure A1 in the Appendix). In separate experiments, EIS experiments were conducted from 20 kHz down to 2±1 mHz. At different DC potentials, the AC potential was set to 8 mV_{rms}, and the data was acquired with an average of 10±2 points per decade. In the experimental setup, all electrochemical measurements, including OCP, potentiodynamic sweeps, and EIS were performed using a Gamry Interface 1010b™[†] potentiostat.

[(4)] The purpose of isolating the counter electrode in a separate chamber is to prevent the byproducts or side reactions at the counter electrode from contaminating or interfering with the desired reaction at the working electrode.

[(5)] The oxygen level was not directly measured in these measurements but referring to previous experiments conducted with the same test apparatus, by using the same procedures, the oxygen level is typically measured to be approximately 1 ppb (maximum 3 ppb), as documented by Kahyarian, et al., in their study on the electrochemistry of CO_2 corrosion of mild steel.[10]

[†] Trade name.

RESULTS AND DISCUSSION

4.1 | Effect of Chloride Ion on the Anodic Dissolution of Iron in Strong Acid Solutions

Years of study on the mechanism of anodic iron dissolution in acidic environments showed that the role of anions such as halides, etc., is not only limited to being a supporting electrolyte, as they can participate in the reaction and change the electrochemical mechanism.[17,20,22-25,30] Figure 6 shows the anodic potentiodynamic sweeps in strong acid chloride and sulfate solutions at pH 4.0. The anodic current density generally decreased in chloride solution compared to sulfate solution. Considering that the only difference between the two solutions is the nature of the anions originating from the added supporting electrolyte and the acid, it can be postulated that the presence of different anions is the reason behind the increase or decrease of the current density.

As discussed above, the studies in the open literature reported that halides (in our case chlorides) can participate in the anodic reaction by replacing OH^- on the iron surface through competitive adsorption.[17,20,22-24,30] These studies suggested that the adsorbed chlorides form complexes with iron that somehow participate in the mechanisms of iron dissolution, along with the adsorbed hydroxide intermediates.

Generally, the observed change in the anodic current density in the presence of chlorides can be interpreted by using one of the following three hypotheses:

(1) The total anodic current density is obtained as the sum of the two partial current densities. One comes from the anodic reaction occurring on the fraction of the surface involving adsorbed hydroxide complexes and the other partial coming from the part of the surface involving adsorbed chloride complexes. Hence, the total anodic current density depends on the relative contributions of the two partial current densities. As studies suggested that the hydroxide-catalyzed reactions are faster, producing more current,[17] once they are partially replaced by the chloride intermediates, the total anodic current density decreases. For this scenario, one can expect that an EIS spectrum would show one more time constant in chloride solutions compared to a sulfate solution, due to the additional reaction path involving the adsorbed chloride intermediates, whereas the parts of the spectrum that are associated with the hydroxide intermediates would remain largely unchanged.

(2) Adsorbed hydroxide complexes were identified in the mechanism of iron dissolution in sulfate solutions. However, in chloride solution, the nature of these adsorbed hydroxide complexes changes, leading to alterations in the kinetic constants that govern the iron dissolution reaction sequence.[21] The result is a deceleration of anodic current density when chlorides are involved. In this scenario, one can expect that an EIS spectrum would show the same number of time constants in both sulfate and chloride solutions due to the same number of reaction paths. In addition, the EIS spectrum would have different characteristics as the nature of the adsorbed intermediate complexes, and the kinetic constants associated with it have changed.

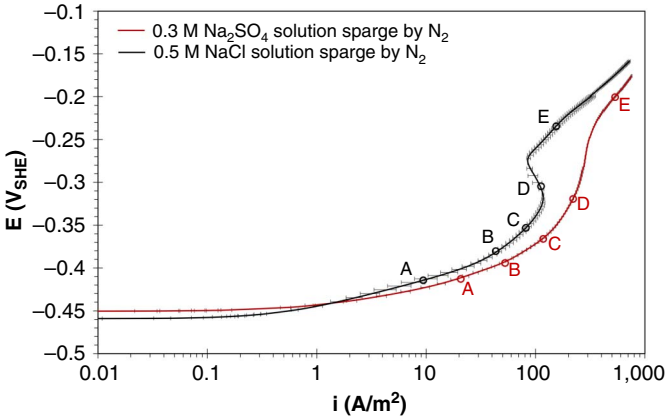

FIGURE 6. *Comparison between the anodic steady-state potentiodynamic sweep curves in strong acid solutions measured using sweep rates of 0.5 mV/s for NaCl solution and 0.125 mV/s for Na_2SO_4 solution on 99.99 wt% pure iron RDE at 1,600 rpm, corroding in an aqueous solution at pH 4.0 and 25°C. The alphabetic letters show the DC potential at which EIS measurements were conducted.[6] Error bars represent minimum and maximum values obtained in repeated experiments.*

(3) Both scenarios above play out at the same time. In that case, the EIS spectrum should show an additional time constant in chloride solutions, due to an additional pathway, with the characteristics of the other parts of the spectrum qualitatively changing as well, due to the changes like the adsorbed intermediate complexes.

To elucidate the role of chloride on the mechanism of iron dissolution, EIS spectra were collected at different DC potentials, indicated on the anodic potentiodynamic sweeps (Figure 6) by letters A, B, C (in the active dissolution region), D (in the transition region), and E (in the prepassivation region) respectively. EIS results obtained in the strong acid solution are shown in Figures 7 through 9.

In all Nyquist plots shown below, the high-frequency (~10^1 Hz to 10^4 Hz) capacitive loop is assumed to be related to the double-layer capacitance that is in parallel with the charge transfer resistance and will not be the focus of the following discussion. In the active dissolution region, at DC potentials A and B (see Figure 6), the two Nyquist plots are presented in Figure 7; in both sulfate and chloride solutions, we can see three loops marked by letters a, b, and c. According to EIS theory, only adsorbed species can display both inductive and capacitive loops depending on the potential and the kinetics of reactions.[31] Hence, we speculate that these loops are linked to adsorbed species involved in the iron dissolution mechanism similar to Keddam, et al.,'s assumption.[3-4] The first inductive loop (a), obtained in the frequency range approximately 10^{-1} Hz to 10^1 Hz, is always related to the adsorbed species $Fe(I)_{(ads)}$ being $FeOH_{(ads)}$, i.e., to the time constant associated with path 1 in Keddam, et al.,'s multipath mechanism (refer to Figures 3 and 4).[3-4,A1] Loop (b) typically seen in the frequency range approximately 10^{-2} Hz to 10^{-1} Hz, could then be related to another intermediate adsorbed species $Fe(I)^*_{(ads)}$ being $Fe(FeOH)_{(ads)}$ that is part of path 2 in Keddam, et al.'s mechanism for iron dissolution.[3-4] According to Keddam, et al., loop c observed at very low frequency approximately 10^{-3} Hz to 10^{-2} Hz is due to adsorbed hydrogen and is expected to fade away at higher current density (above 200 A/m^2).[3]

[6] There are some uncertainties regarding the measured solution resistance in these experiments which were not fully resolved, due to raw data which could not be recovered.

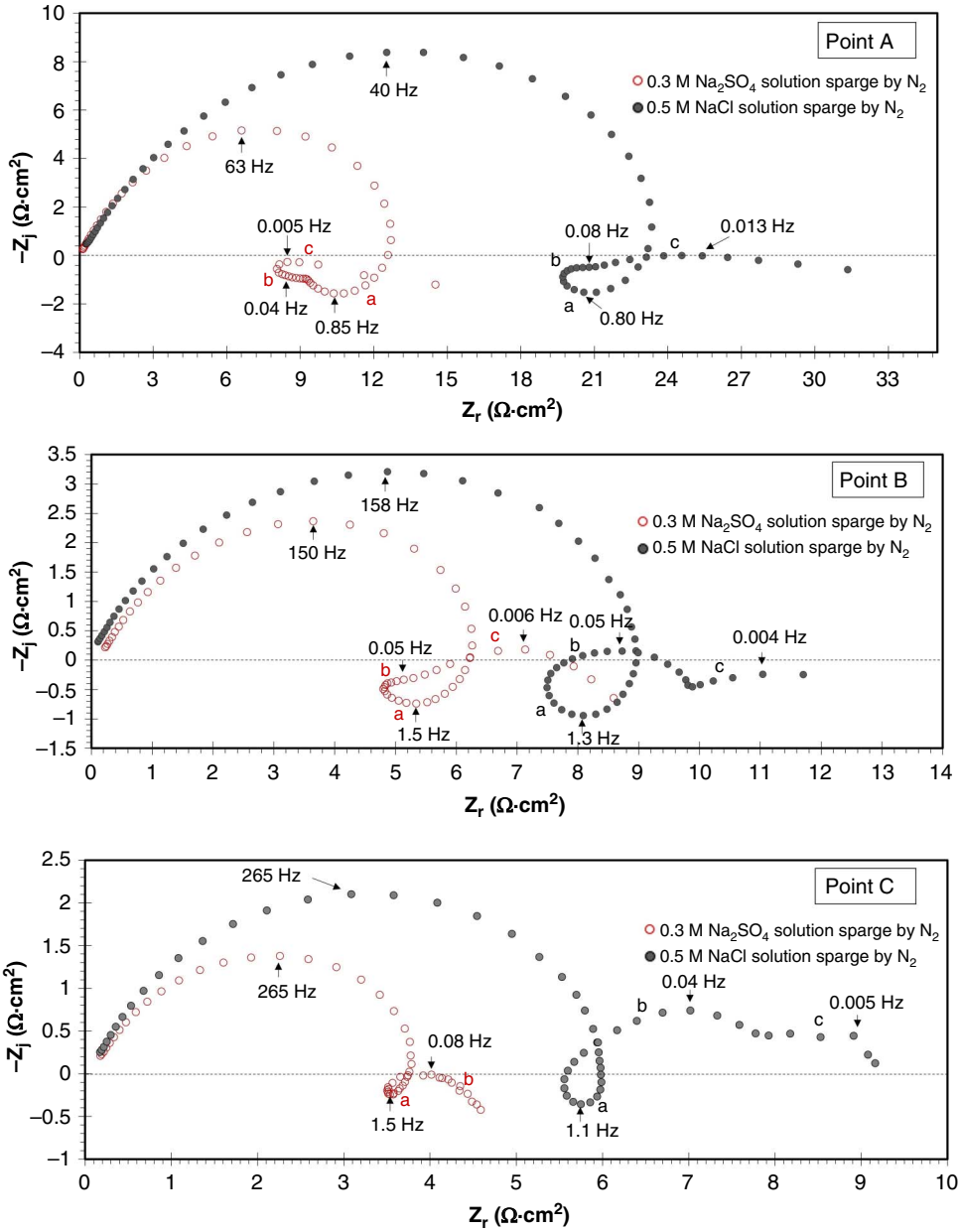

FIGURE 7. *Nyquist plots obtained in the active dissolution region at various potentials marked on the steady-state potentiodynamic sweeps shown in Figure 6. Experimental parameters: 1 bar N_2, 0.3 M Na_2SO_4, or 0.5 M NaCl, pH 4.0, 25°C, 99.99 wt% pure iron RDE, 1,600 rpm.*[7]

At a more positive potential (point C in Figure 6), the Nyquist plot shown in Figure 7 obtained in sulfate solution shows two loops a and b while loop c disappeared, just as Keddam, et al., suggested would happen.[3-4] However, in chloride solution third loop c is observed. The presence of the additional loop c in chloride solution might be due to two different possibilities:

- The presence of adsorbed hydrogen on the iron surface which dissipated in sulfate solutions was still there in chloride solution and might disappear at more positive potential and current density.[3]
- The presence of an additional adsorbate with a different reaction path in a chloride solution compared to the sulfate solution, which should not dissipate at more positive potential and current density.

The first possibility is supported by one fact seen in Figure 7, the frequency range approximately 10^{-3} Hz to 10^{-2} Hz, where loop c appeared in chloride solutions at the more positive potential (point C in Figure 6) is the same as it was at the more negative potentials (points A and B in Figure 6). On the other hand, the second scenario is consistent with the studies reporting that halides can participate in the anodic reaction by replacing OH^- on the iron surface through competitive adsorption and forming complexes with iron.[17,20,22-24,30] Further analysis of the impedance response at more positive potentials (discussed below) suggests that loop c might be associated with an adsorbed complex species formed in the presence of chloride ions and participating in the anodic reaction.

[7] Reproducibility of the EIS data are shown in Figures A2, A6, and A7 in the Appendix.

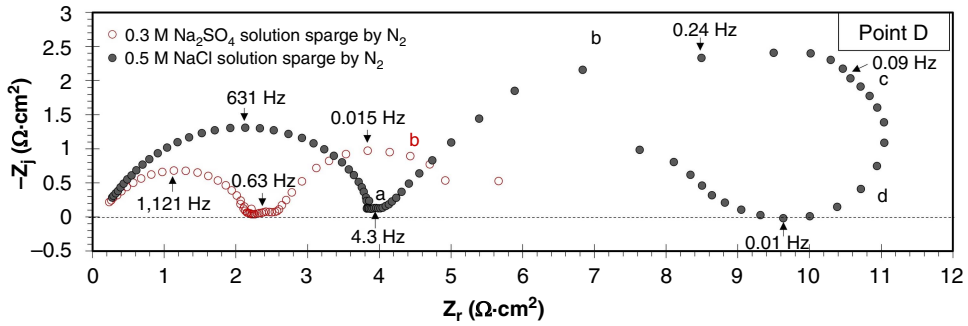

FIGURE 8. *Nyquist plots obtained in the transition region (D) marked on the steady-state potentiodynamic sweeps shown in Figure 6. Experimental parameters: 1 bar N_2, 0.3 M Na_2SO_4, or 0.5 M NaCl, pH 4.0, 25°C, 99.99 wt% pure iron RDE, 1,600 rpm.*[8]

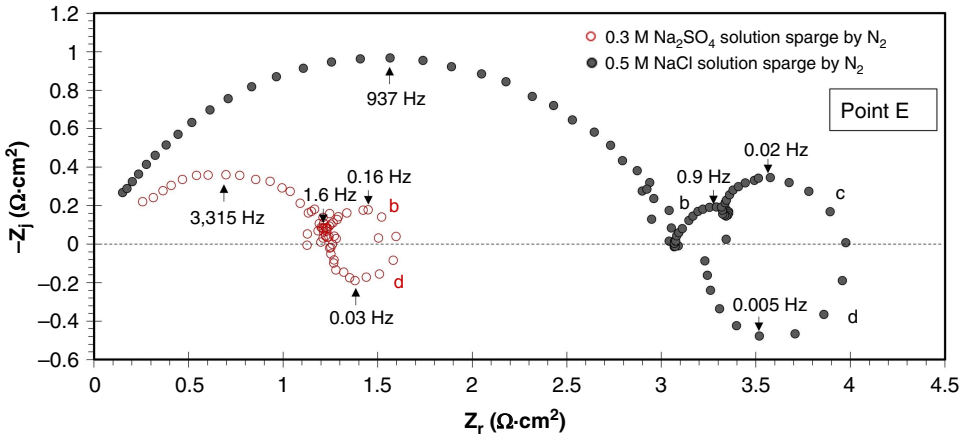

FIGURE 9. *Nyquist plots obtained in the prepassivation region (E) marked on the steady-state potentiodynamic sweeps shown in Figure 6. Experimental parameters: 1 bar N_2, 0.3 M Na_2SO_4, or 0.5 M NaCl, pH 4.0, 25°C, 99.99 wt% pure iron RDE, 1,600 rpm*[9].

Figure 8 shows the Nyquist plot at DC potentials in the transition region (point D in Figure 6). The Nyquist plot obtained in the sulfate solution shows two loops a and b at low frequency which are thought to be the same as those seen at more negative potentials in the active dissolution region, i.e., that they are related to path 1 and path 2, respectively, in Keddam, et al.,'s mechanism for iron dissolution (refer to Figures 3 and 4).[3-4] However, the Nyquist plot obtained in the chloride solution shows four loops (a, b, c, and d)[10].

In both solutions, for the transition region, loop a has significantly shrunk and shows up over a narrow range of frequencies. It has also changed from an inductive loop seen in the active dissolution region (Figure 7) to a capacitive loop in the transition region (Figure 8). It is thought that both the inductive and capacitive loops a are associated with the same species and reaction path, i.e., species $Fe(I)_{(ads)}$ or $FeOH_{(ads)}$ that is part of path 1 in Keddam, et al.,'s mechanism,[3-4] as judged by the similar magnitude of the characteristic frequency (~10^0 Hz) related to the time constant of each loop. Due to the change in potential and the kinetics of different steps in the same reaction path, the impedance response in terms of the Nyquist plot, can present itself as an inductive or capacitive loop.[31]

In Figure 8, looking at the spectrum obtained for the transition potential region (point D), we can find two additional loops c and d in the low-frequency potential region for chloride solutions that are not present in sulfate solutions. If we think of the transition region in terms of Keddam, et al.,'s mechanism as the potential range where there is a change in the contribution of anodic reaction pathways (For example, in Figure 5, the contribution of anodic reaction path 1 decreases in the transition region, while the contributions of paths 2 and 3 increase), we can assume that one of these two loops (c or d), seen in chloride solutions is related to path 3 in Keddam, et al.,'s mechanism (refer to Figures 3 and 4), i.e., that it involved the intermediate adsorbed complex $Fe(II)^*_{(ads)}$ which according to the analysis above, could be $Fe(Fe(OH)_2)_{(ads)}$. Then the question is, why is neither of these two loops observed in the Nyquist plot obtained in the sulfate solution shown in Figure 8? One possible explanation can be found by looking at the steady-state potentiodynamic sweeps shown in Figure 6 for the two solutions, where a much broader, less pronounced transition region is seen for the sulfate solution compared to the chloride solution. Therefore, it was harder to properly select a potential (point D) in the sulfate solution which would effectively bring out the various reaction paths and intermediate complex adsorbates

[8] Reproducibility of the EIS data are shown in Figures A3 and A7 in the Appendix.

[9] Reproducibility of the EIS data in chloride solution is shown in Figure A3 in the Appendix.

[10] In chloride solutions, the potentiodynamic sweep in the transition region (point D in Figure 6) has a "negative slope" which should result in a negative polarization resistance. However, the Nyquist plot at this DC potential shows a positive real part at very low frequency (Figure 8). A reason for not observing impedance data with a negative real part might be due to the difficulty in reproducing the exact potential where the DC current density is reversed (has a local maximum). In addition, the measurements of the impedance data in a potential range where the polarization resistance has a negative value are very difficult and sensitive to the instability of the DC current density. Therefore, measuring the impedance data with negative polarization resistance cannot always be achieved.

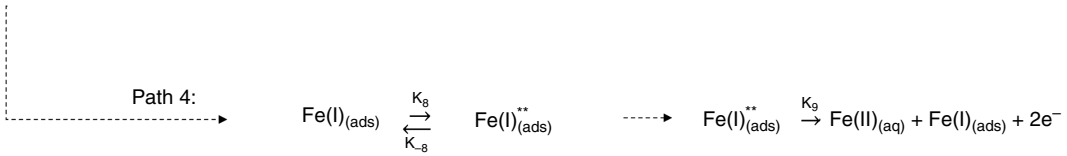

FIGURE 10. *Additional reaction path for iron dissolution in strong acid solutions due to the presence of chlorides, based on the reconstructed multipath mechanism for iron dissolution of Keddam, et al.,[3-4] shown in Figure 3.*

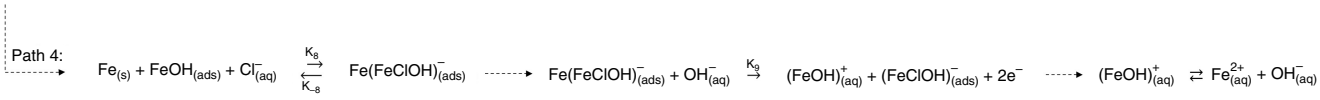

FIGURE 11. *Additional reaction path for iron dissolution in strong acid solutions due to the presence of chlorides to the one shown in Figure 4, based on Keddam, et al.,[3-4] using equivalent species with an exact chemical composition deduced by analogy with the catalytic (Heusler) mechanism.[14]*

typical for the transition region. At potentials more negative than the one selected for point D in sulfate solutions, we see loops associated with an active dissolution of iron (as with points A, B, and C), while at more positive potentials (as with point E) we observe loops associated with pre-passivation as shown in Figure 9. Even if we assume that one of the two additional loops (c or d) seen only in chloride solutions is related to path 3 in Keddam, et al.'s mechanism, there is one additional loop that needs to be accounted for in the Nyquist plot for the transition region, shown in Figure 8. This indicates that there is one additional reaction path and one additional adsorbed intermediate species participating in the iron dissolution reaction in strongly acid chloride solution compared to the sulfate solution.

Figure 9 shows the Nyquist plots for the prepassivation region (point E in Figure 6) in strong acid chloride and sulfate solutions. By comparison with results obtained in the active dissolution region, it appears that loop a related to path 1 in Keddam, et al.'s mechanisms, which was barely distinguishable in the transition region, has disappeared altogether for the pre-passivation potential region, in both chloride and sulfate solutions. Moreover, loops b and c, which were hard to distinguish from each other in the transition region separated more clearly at more positive potential in the prepassivation region. Comparing the two Nyquist plots in Figure 9, there is one additional loop in the chloride solution compared to the sulfate solution, indicating that there is one additional adsorbed intermediate species and one more reaction path involved in the iron dissolution.

In summary, the experimental EIS data obtained at different potentials in strong acid solutions showed that there is one additional loop corresponding to one additional reaction path and a different adsorbed intermediate complex involved in the anodic reaction, clearly seen at more positive potential. Therefore, the original multi-path mechanism of Keddam, et al.,[3-4] for sulfate solutions, needs to be extended to explain the behavior of the anodic dissolution of iron in strong acid solutions containing chlorides.

Revisiting the three hypotheses that were postulated above about the possible role of chlorides, we can conclude that it is the first one that is confirmed, i.e., that the total anodic current density is a sum of partial current densities, one involves the adsorbed hydroxide complexes and the other involves the adsorbed chloride complex. This is based on the EIS spectra

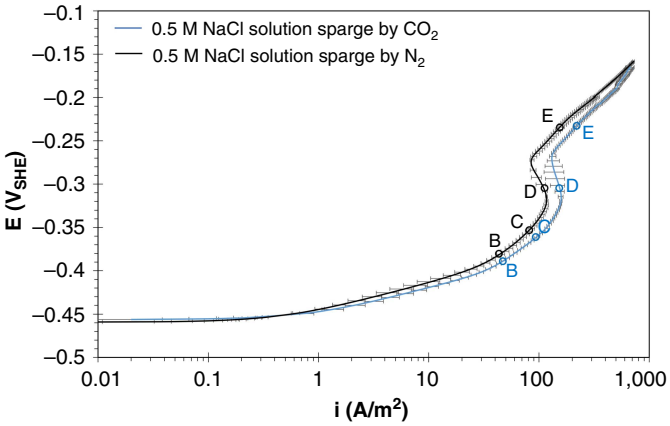

FIGURE 12. *Comparison between the anodic steady-state potentiodynamic sweep curves in chloride solution sparged with 1 bar CO_2 or N_2, measured using a sweep rate of 0.5 mV/s, on 99.99 wt.% pure iron RDE at 1,600 rpm, corroding in an aqueous solution at pH 4.0 and 25°C.[11] Error bars represent minimum and maximum values obtained in repeated experiments.*

(shown in Figures 7 through 9) that show one more time constant in chloride solutions compared to sulfate solutions, while the other parts of the spectra that are associated with the hydroxide intermediates do not qualitatively change. In other words, in chloride solutions, we saw evidence of the three iron dissolution paths as proposed in Keddam, et al.,'s mechanism (refer to Figures 3 and 4),[3-4] which is the same as in sulfate solutions, as well as an additional path involving chlorides. By analogy with the other two hydroxide-catalyzed pathways in Keddam, et al.,'s mechanism, we can here propose an additional path, where chlorides play the same catalytic role as hydroxide does as shown by Reactions (29) through (32).

$$Fe_{(s)} + OH^-_{(aq)} \rightarrow FeOH_{(ads)} + e^- \quad (29)$$

$$Fe_{(s)} + FeOH_{(ads)} + Cl^-_{(aq)} \rightleftarrows Fe(FeClOH)^-_{(ads)} \quad (30)$$

$$Fe(FeClOH)^-_{(ads)} + OH^-_{(aq)} \rightarrow (FeOH)^+_{(aq)} + (FeClOH)^-_{(ads)} + 2e^- \quad (31)$$

$$(FeOH)^+_{(aq)} \rightleftarrows Fe^{2+}_{(aq)} + OH^-_{(aq)} \quad (32)$$

[11] There are some uncertainties regarding the measured solution resistance in these experiments which were not fully resolved, due to raw data which could not be recovered.

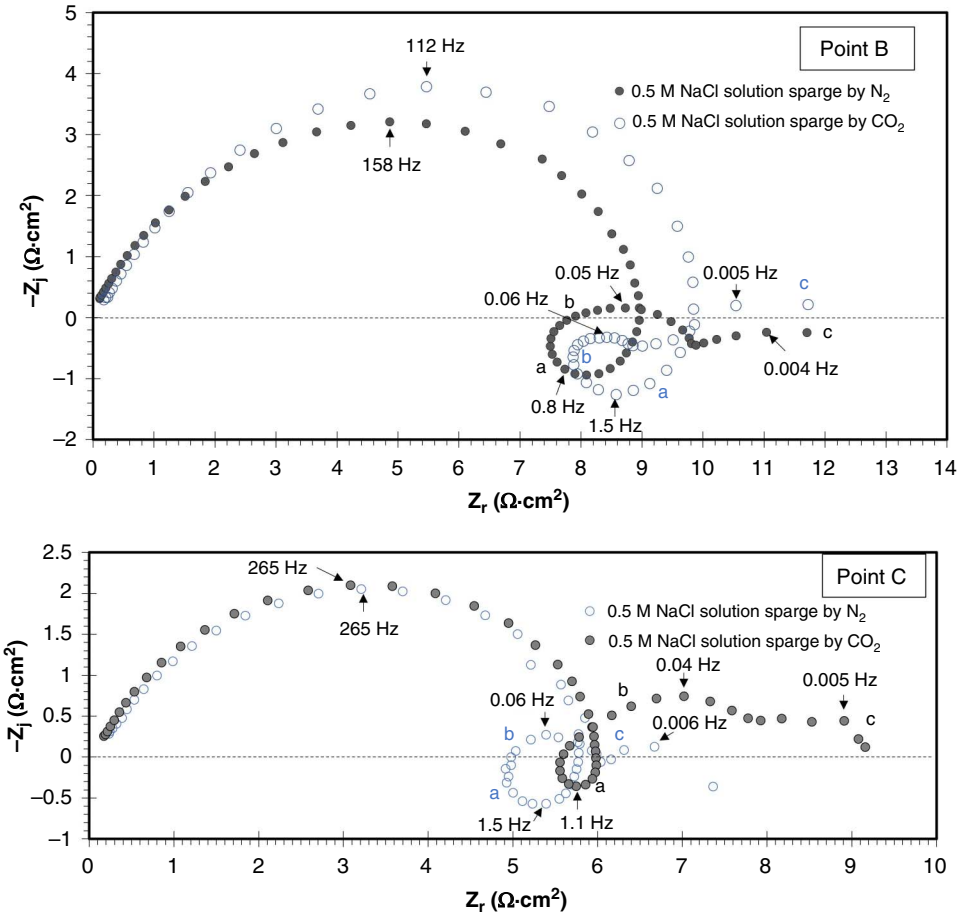

FIGURE 13. *Nyquist plots obtained in the active dissolution regions (B and C) marked on the steady-state potentiodynamic sweeps shown in Figure 12. Experimental parameters: 1 bar N_2 or 1 bar CO_2, 0.5 M NaCl, pH 4.0, 25°C, 99.99 wt% pure iron RDE, 1,600 rpm*[12].

According to this mechanism, the chloride containing catalytic species is $Fe(FeClOH)^-_{(ads)}$, formed by Reaction (30) and the whole reaction sequence (29) through (32) can be considered to be path 4 that needs to be added to Keddam, et al.,'s mechanism.[3-4] Using the original notation of Keddam, et al., the additional reaction path can be written as shown in Figure 10 or we can spell out the likely chemical composition of the species involved, deduced by analogy with the catalytic (Heusler) mechanisms,[14] and write stoichiometrically correct reaction steps, and the additional reaction path as shown in Figure 11.

The proposed mechanism is reminiscent of the one put forward by MacFarlane and Smedley,[22] which was also based on the Keddam, et al.,[3-4] mechanism. The distinction lies in MacFarlane and Smedley's assumption, where chloride intermediate species are assumed to form directly through the reaction of chlorides and hydroxide ions with iron (Reaction [23]). In contrast, our proposed mechanism suggests that the initial step involves the formation of $FeOH_{(ads)}$, followed by a subsequent chemical reaction with Cl^- which leads to the formation of the adsorbed chloride intermediate. Furthermore, this chloride intermediate is regarded as a catalyst for the final reaction step, whereas this catalytic role is not present in the mechanism proposed by MacFarlane and Smedley.

4.2 | Effect of Aqueous CO_2 on the Anodic Dissolution of Iron

The present study also investigated the mechanism of iron dissolution in aqueous CO_2 solutions. Once CO_2 dissolves in water, it is hydrated and produces a weak carbonic acid H_2CO_3, which dissociates to give bicarbonate ions HCO_3^- and carbonate ions CO_3^{2-}. The question is whether any of these aqueous carbonic species might influence the mechanism and kinetics of anodic dissolution of iron.

A first answer to the question can be found in Figure 12, which shows steady-state anodic potentiodynamic sweeps in strong acid chloride solution (sparged by 1 bar N_2) and weak acid chloride solution (saturated with 1 bar CO_2). Results show that the rate of iron dissolution was increased in aqueous CO_2 environments compared to the strong acid solution. To investigate the reasons for this behavior, EIS measurements were performed at DC potentials B, C, D, and E to study the anodic dissolution of iron in aqueous CO_2 environments.

Figures 13 and 14 illustrate the impedance response of iron dissolution in strong acid and weak acid CO_2 solutions, at DC potentials B, C, D, and E marked in Figure 12. In all cases, the first high-frequency loop is assumed to be related to the response of the double-layer capacitance in parallel with the charge transfer resistance, and will not be discussed in any detail. In the Nyquist plots at DC potentials B and C (Figure 13), set in the active dissolution potential region, there are three loops marked by letters a, b, and c, in both strong acid chloride solution and

[12] Reproducibility of the EIS data are shown in Figures A2 and A4 in the Appendix.

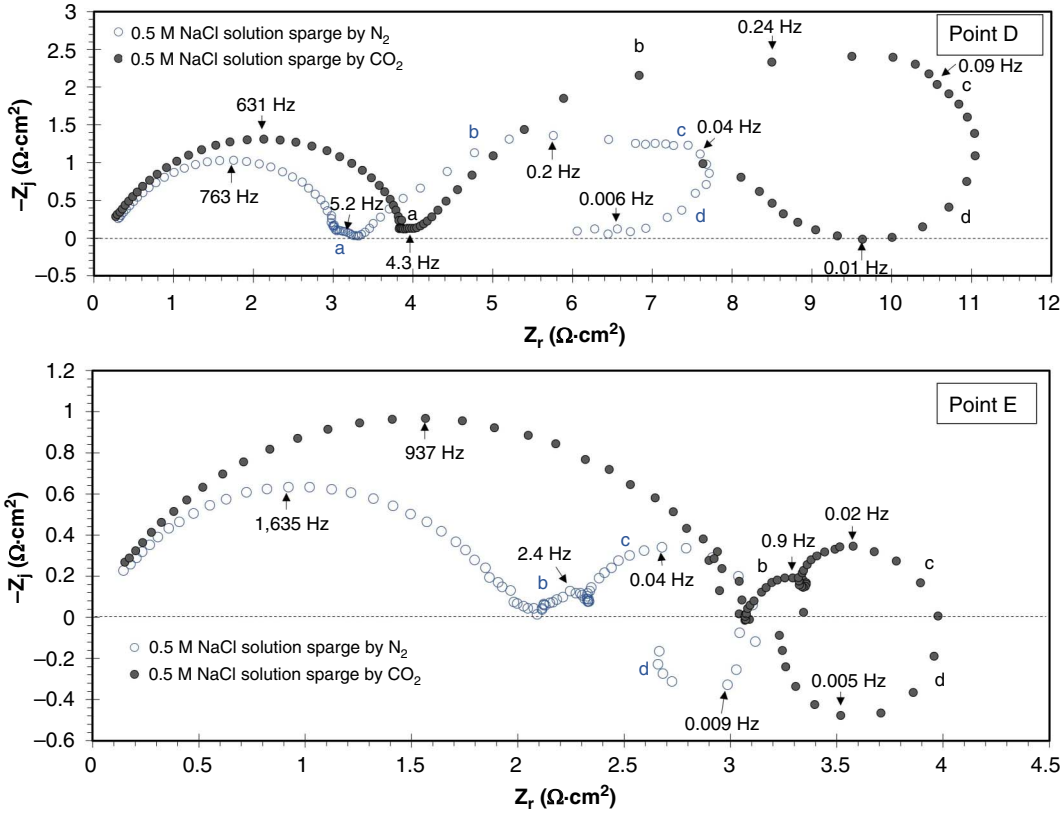

FIGURE 14. *Nyquist plots obtained in the transition region (D) and prepassivation region (E) marked on the steady-state potentiodynamic sweeps shown in Figure 12. Experimental parameters: 1 bar N_2 or 1 bar CO_2, 0.5 M NaCl, pH 4.0, 25°C, 99.99 wt% pure iron RDE, 1,600 rpm*[14].

weak CO_2 solution. These observations indicate that, in both solutions, there are three adsorbed species involved and three distinct reaction paths in the mechanism of iron dissolution in the active dissolution region, acting in approximately the same way, i.e., that there was little or no change caused by the introduction of CO_2 into the aqueous solution.

At more positive potential, the Nyquist plots at DC potential D set in the transition potential region (Figure 14), show four loops a, b, c, and d[13] in both solutions. Their characteristics appear to be the same. This observation indicates that there are the same number of reaction paths and adsorbed intermediate complexes involved in the mechanism of iron dissolution in an acidic solution, irrespective of the presence of dissolved CO_2. Although the two loops b and c are not quite decoupled at this potential, experiments at a more positive DC potential E, set in the pre-passive potential region (Figure 14) show that, at higher current density, these two loops are clearly distinguished due to the change in their characteristic frequencies. At this potential, the number of loops and their similar appearance once again indicate the same number of reaction pathways and adsorbed intermediate species in the two solutions.

Based on the impedance response, we can conclude that, unlike chlorides, aqueous carbonic species do not lead to additional reaction pathways for iron dissolution. Therefore, in aqueous CO_2 solutions containing chlorides, we can consider that the anodic mechanism follows the same multipath mechanism that was proposed for the anodic dissolution of iron in chloride-containing strong acid solutions, as described above. However, we cannot ignore the fact that the kinetics of the iron dissolution reaction is higher in CO_2 aqueous environments compared to the strong acid solution, as shown in Figure 12. The reason for this could be a change in the solution composition close to the metal surface including a buffered more acidic pH.[11,32] This and the presence of carbonic species may also lead to a change in the nature and chemical composition of the adsorbed intermediate complexes (both hydroxides and chlorides), which affects the kinetic rate constant of the multistep reactions. It is also possible that there is a change in the extent of coverage of the surface by different adsorbed intermediate species and ions.

A parallel ToF-SIMS in-depth profiling and 3D mapping study was conducted under similar conditions as were used in the present EIS study. The results are presented in Part II of this paper series.[12] This experimental technique detected adsorbed hydroxide and chloride intermediates formed during the iron dissolution process, which is consistent with the multipath reaction mechanism proposed here. Despite the presence of aqueous carbonic species and their observed effect on the kinetics of iron dissolution, no additional adsorbed intermediates have been detected in aqueous CO_2 environments, indicating that carbonic species do not directly participate in the iron dissolution reaction.

CONCLUSIONS

➢ The present study showed that the rate of anodic dissolution of iron decreases in the presence of chlorides.

[13] Note that loop "a" is transformed from inductive the loop at DC potential C (Figure 13) to a capacitive loop in DC potential D (Figure 14). During the transition the capacitive loop collapsed and can hardly be distinguished.

[14] Reproducibility of the EIS data are shown in Figures A3 and A5 in the Appendix.

➢ Based on analysis of EIS data and interpretation of Nyquist plots, it is evident that adsorption of chloride ions results in the formation of additional intermediate complexes, which participate in the anodic reaction through a distinct reaction path in addition to those present in strong acid sulfate solutions.
➢ Through examination of Nyquist plots, it is determined that the presence of aqueous CO_2 does not lead to new reaction paths for anodic dissolution of iron even if the rate of iron dissolution accelerates in the presence of CO_2. This could be due to the change in the solution composition at the metal surface, including a lower pH, which may lead to a change in the nature and chemical composition of the adsorbed complexes (both hydroxides and chlorides) with different kinetic constants and extent of surface coverage.

ACKNOWLEDGMENTS

The authors would like to acknowledge the financial support from the following companies: Ansys, Baker Hughes, Chevron Energy Technology, Clariant Corporation, CNOOC, ConocoPhillips, ExxonMobil, M-I SWACO (Schlumberger), Multi-Chem (Halliburton), Occidental Oil Company, Pertamina, Saudi Aramco, Shell Global Solutions, and TotalEnergies.

References

1. A. Kahyarian, S. Nesic, *J. Electrochem. Soc.* 166 (2019): p. C3048-C3063.
2. J.O. Bockris, D. Drazic, A.R. Despic, *Electrochim. ica Acta* 4 (1961): p. 325-361.
3. M. Keddam, O.R. Mottos, H. Takenouti, *J. Electrochem. Soc.* 128 (1981): p. 257.
4. M. Keddam, O.R. Mattos, H. Takenouti, *J. Electrochem. Soc.* 128 (1981): p. 266.
5. G. Ogundele, W. White, *Corrosion* 42 (1986): p. 71-78.
6. S. Nesic, J. Postlethwaite, S. Olsen, *Corrosion* 52 (1996): p. 280-294.
7. K.S. George, S. Nesic, *Corrosion* 63 (2007): p. 178-186.
8. L.G.S. Gray, B.G. Anderson, M.J. Danysh, P.R. Tremaine, "Mechanisms of Carbon Steel Corrosion in Brines Containing Dissolved Carbon Dioxide at pH 4," CORROSION 89, paper no. 40 (Houston, TX: NACE, 1989).
9. D.H. Davies, G.T. Burstein, *Corrosion* 36 (1980): p. 416-422.
10. A. Kahyarian, B. Brown, S. Nesic, *Corros. Sci.* 129 (2017): p. 146-151.
11. B.R. Linter, G.T. Burstein, *Corros. Sci.* 41 (1999): p. 117-139.
12. L. Wang, H. Wang, N. Moradighadi, A. Seyeux, P. Alain, S. Nesic, P. Marcus, *Corrosion*, 80 (2024): p. 724-733.
13. A.A. El Miligy, D. Geana, W.J. Lorenz, *Electrochem. Acta* 20 (1975): p. 273-281.
14. K.E. Heusler, *Z. Elektrochem. Berichte Der Bunsengesellschaft Phys. Chem.* 62 (1958): p. 582-587.
15. I. Epelboin, M. Keddam, *J. Electrochem. Soc.* 117 (970): p. 1052.
16. A.J. Bard, L.R. Faulkner, *Electrochemical Methods: Fundamentals and Applications*, 2nd ed. (New York, NY: John Wiley & Sons, Inc., 2001), p. 95.
17. D.M. Dražić, "Iron and Its Electrochemistry in an Active State," in *Modern Aspects of Electrochemistry*, eds. B.E. Conway, J.O. Bockris, R.E. White (Boston, MA: Springer US, 1989), p. 69-192.
18. P. Marcus, *Corrosion Mechanisms in Theory and Practice*, Third Edition (Boca Raton, FL: CRC Press, 2011), p. 173-174.
19. A.Yu. Aleksanyan, I.I. Reformatskaya, A.N. Podobaev, *Prot. Met.* 43 (2007): p. 125-128.
20. K.E. Heusler, G.H. Cartledge, *J. Electrochem. Soc.* 108 (1961): p. 732.
21. O.E. Barcia, O.R. Mattos, *Electrochim. Acta* 35 (1990): p. 1003-1009.
22. D.R. MacFarlane, S.I. Smedley, *J. Electrochem. Soc.* 133 (1986): p. 2240.
23. N.A. Darwish, F. Hilbert, W.J. Lorenz, H. Rosswag, *Electrochim. Acta* 18 (1973): p. 421-425.
24. Z.A. Foroulis, *J. Electrochem. Soc.* 113 (1966): p. 532.
25. H.C. Kuo, K. Nobe, *J. Electrochem. Soc.* 125 (1978): p. 853.
26. S. Nesic, N. Thevenot, J.L. Crolet, D. Drazic, "Electrochemical Properties of Iron Dissolution in the Presence of CO_2—Basics Revisited," CORROSION 96, paper no. 96003 (Houston, TX: NACE, 1996).
27. T. das Chagas Almeida, M.C.E. Bandeira, R.M. Moreira, O.R. Mattos, *Corros. Sci.* 120 (2017): p. 239-250.
28. T. Hurlen, S. Gunvaldsen, R. Tunold, F. Blaker, P.G. Lunde, *J. Electroanal. Chem. Interfacial Electrochem.* 180 (1984): p. 511-526.
29. T.C. Almeida, M.C.E. Bandeira, R.M. Moreira, O.R. Mattos, *Corros. Sci.* 133 (2018): p. 417-422.
30. E. McCafferty, N. Hackerman, *J. Electrochem. Soc.* 119 (1972): p. 999.
31. M.E. Orazem, B. Tribollet, *Electrochemical Impedance Spectroscopy*, 2nd ed. (Hoboken, NJ: John Wiley & Sons, Inc., 2017), p. 226-231.
32. E. Remita, B. Tribollet, E. Sutter, V. Vivier, J. Kittel, *Corros. Sci.* 50 (2008): p. 1433-1440.

APPENDIX

COMPARISON GRAPH OF ANODIC POTENTIODYNAMIC SWEEP CURVES AT DIFFERENT SWEEP RATES

The graph shown in Figure A1 illustrates the comparison between the anodic steady-state potentiodynamic sweep curves measured at sweep rates of 0.125 mV/s and 0.5 mV/s in 0.3 M Na_2SO_4 solution. The data reveal that there is no significant difference in measurements using the two sweep rates.

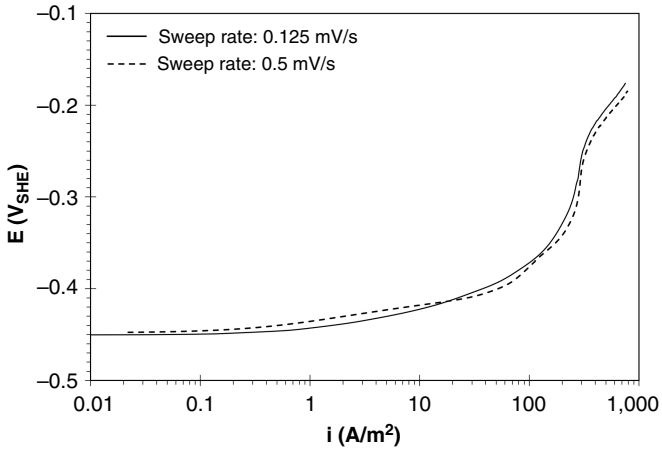

FIGURE A1. *Comparison between the anodic steady-state potentiodynamic sweep curves in strong acid Na_2SO_4 solutions measured using sweep rates of 0.5 mV/s and 0.125 mV/s on 99.99 wt% pure iron RDE at 1,600 rpm, corroding in an aqueous solution at pH 4.0 and 25°C.*[15]

[15] There are some uncertainties regarding the measured solution resistance in these experiments which were not fully resolved, due to raw data which could not be recovered.

REPEATABILITY OF MEASURED ELECTROCHEMICAL IMPEDANCE SPECTROSCOPY DATA

The graph depicted in Figures A2 through A7 illustrates the reproducibility of the EIS data across various DC potentials as discussed in the *Results and Discussion* section of this paper.

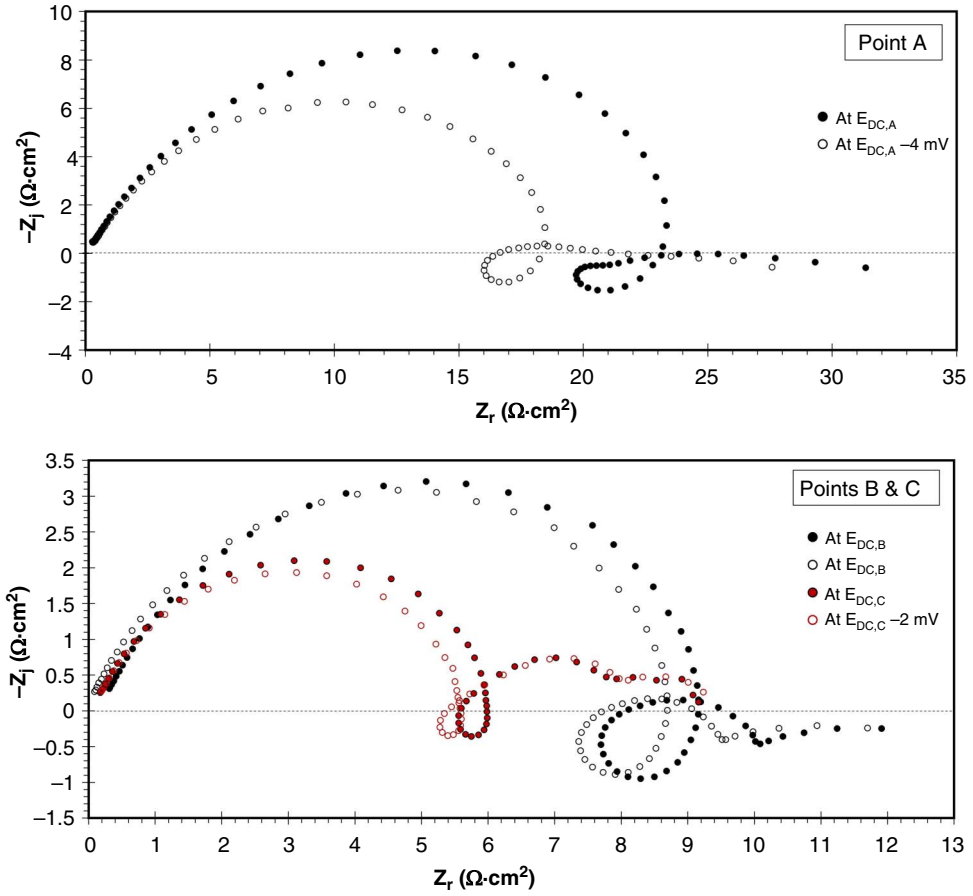

FIGURE A2. *Repeatability of Nyquist plots at approximate DC potentials A to C marked on the steady-state potentiodynamic sweeps shown in Figure 6. Experimental parameters: 1 bar N_2, 0.5 M NaCl, pH 4.0, 25°C, 99.99 wt% pure iron RDE, 1,600 rpm.*

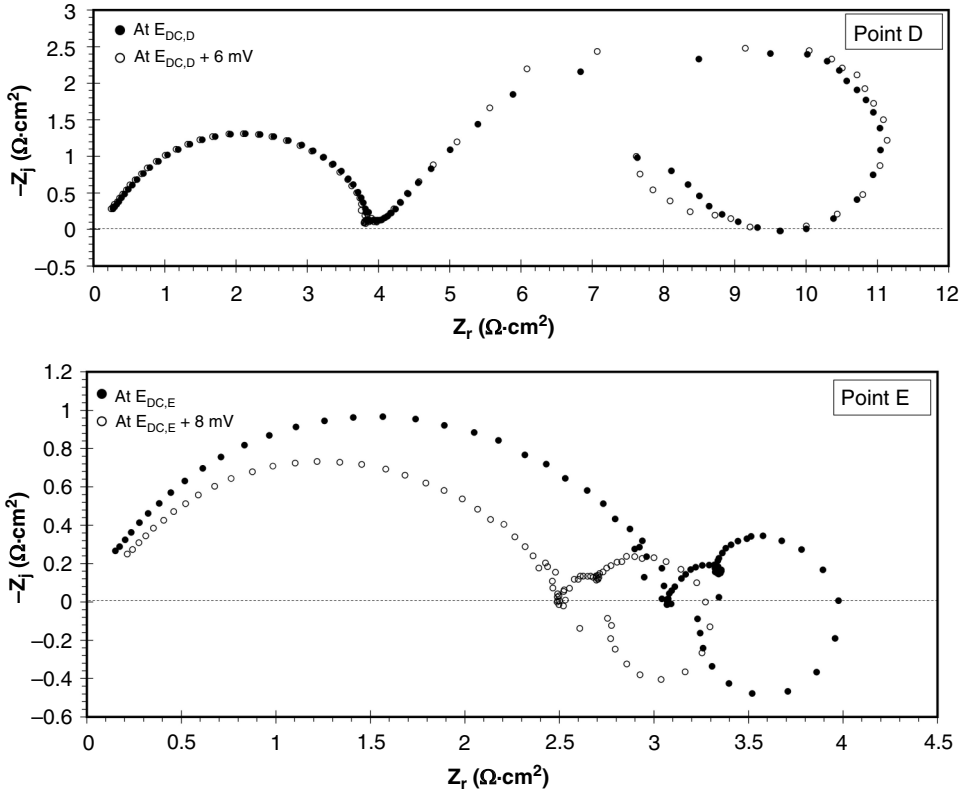

FIGURE A3. *Repeatability of Nyquist plots at approximate DC potentials D and E marked on the steady-state potentiodynamic sweeps shown in Figure 6. Experimental parameters: 1 bar N_2, 0.5 M NaCl, pH 4.0, 25°C, 99.99 wt% pure iron RDE, 1,600 rpm.*

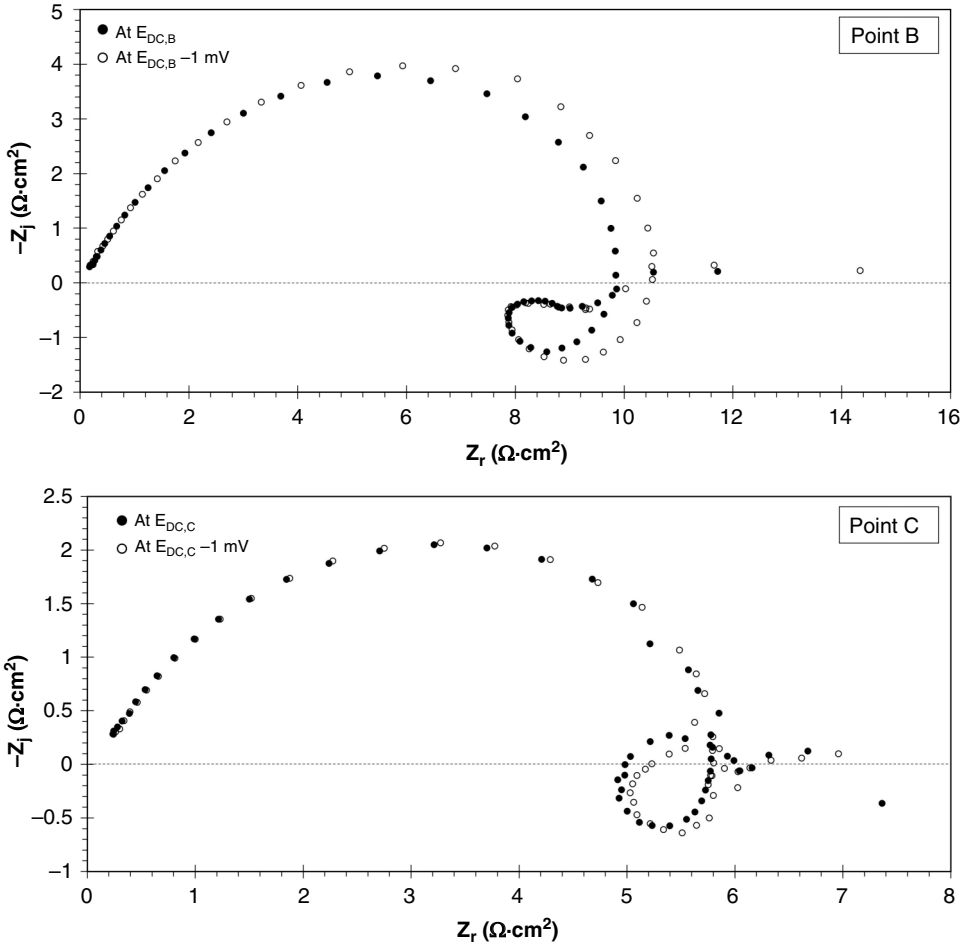

FIGURE A4. *Repeatability of Nyquist plots at approximate DC potentials B and C marked on the steady-state potentiodynamic sweeps shown in Figure 12. Experimental parameters: 1 bar CO_2, 0.5 M NaCl, pH 4.0, 25°C, 99.99 wt% pure iron RDE, 1,600 rpm.*

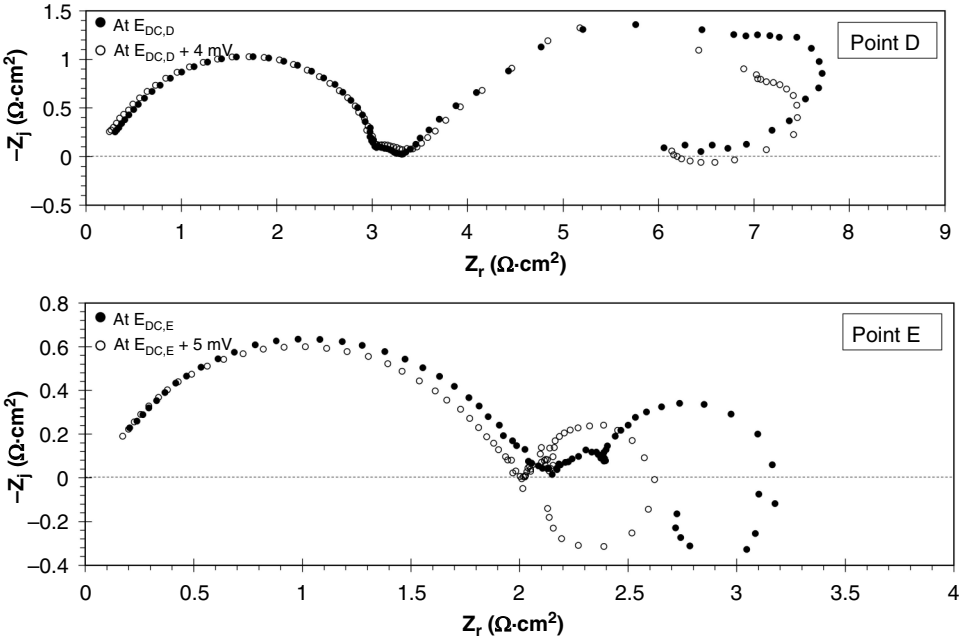

FIGURE A5. *Repeatability of Nyquist plots at approximate DC potentials D and E marked on the steady-state potentiodynamic sweeps shown in Figure 12. Experimental parameters: 1 bar CO_2, 0.5 M NaCl, pH 4.0, 25°C, 99.99 wt% pure iron RDE, 1,600 rpm.*

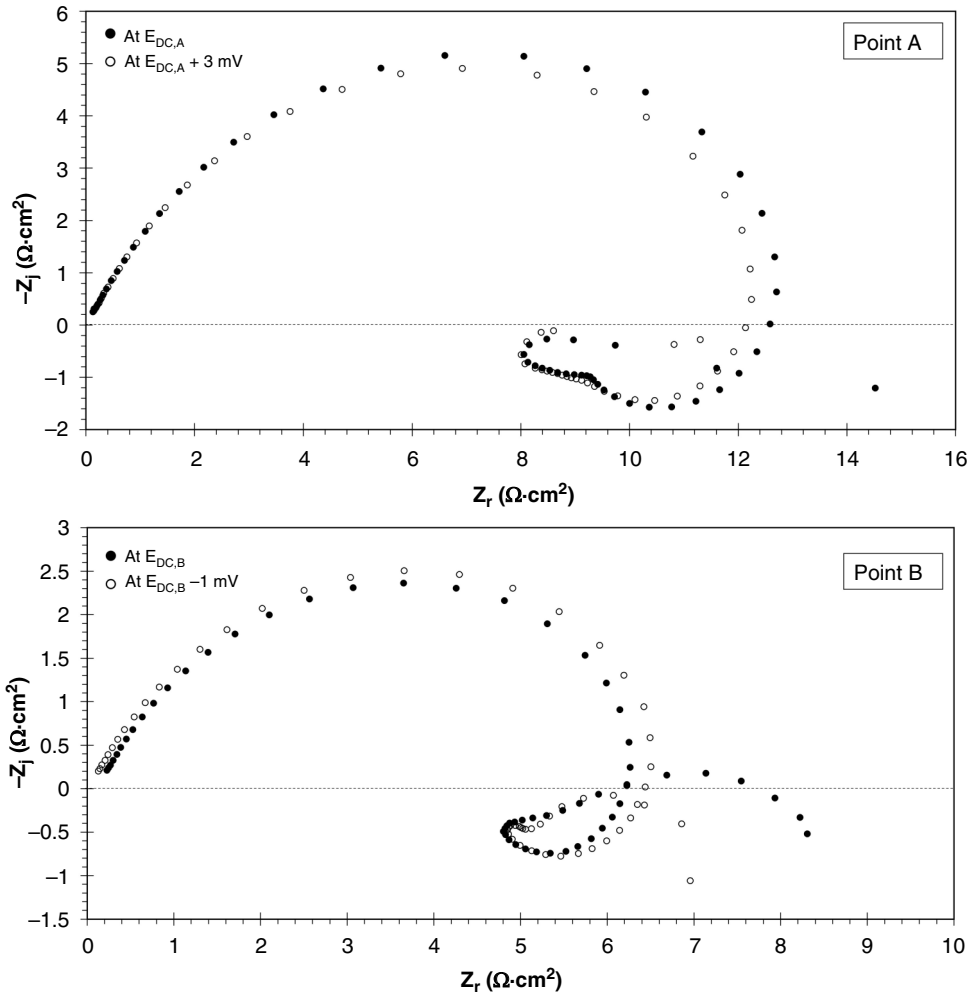

FIGURE A6. *Repeatability of Nyquist plots at approximate DC potentials A and B marked on the steady-state potentiodynamic sweeps shown in Figure 6. Experimental parameters: 1 bar N_2, 0.3 M Na_2SO_4, pH 4.0, 25°C, 99.99 wt% pure iron RDE, 1,600 rpm.*

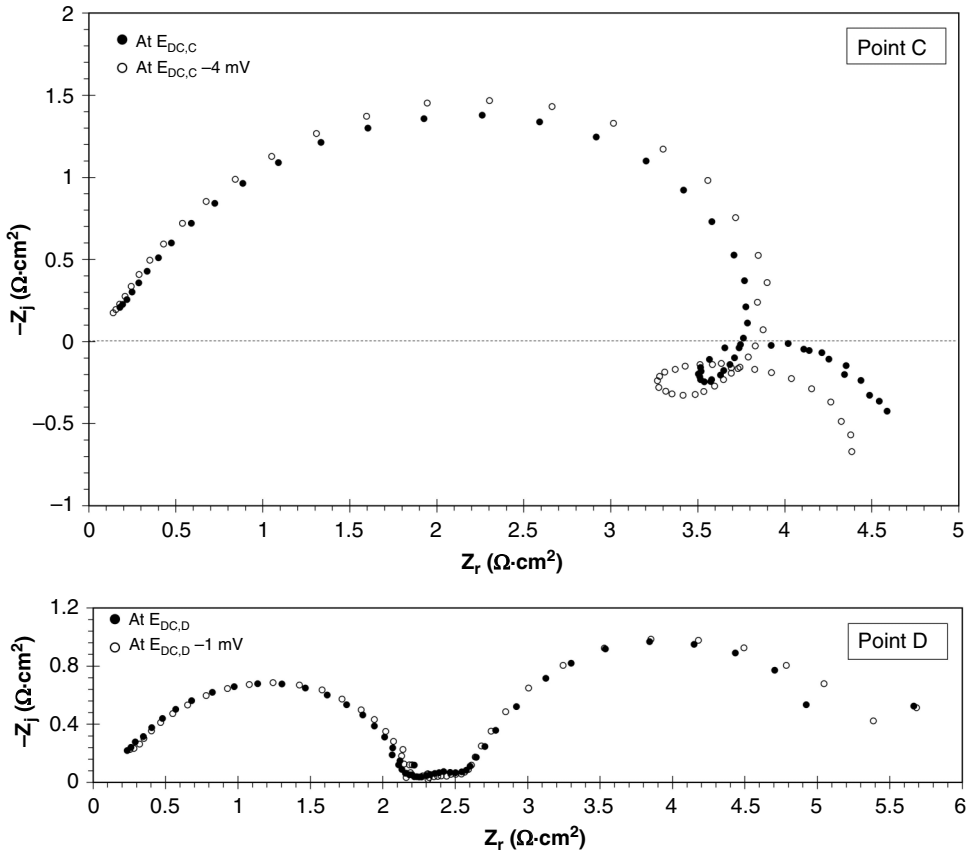

FIGURE A7. *Repeatability of Nyquist plots at approximate DC potentials C and D marked on the steady-state potentiodynamic sweeps shown in Figure 6. Experimental parameters: 1 bar N_2, 0.3 M Na_2SO_4, pH 4.0, 25°C, 99.99 wt% pure iron RDE, 1,600 rpm.*